Shock Waves (1991) 1:149–160

Shock Waves


# Stability of converging cylindrical shock waves

**M. Watanabe and K. Takayama**

Shock Wave Research Center, Institute of Fluid Science, Tohoku University, Katahira 2-1-1 Aoba Sendai JAPAN

Received December 10, 1990; accepted March 3, 1991

**Abstract.** An experrimental and numerical study was made of converging cylindrical shock waves. The goal of the present study was to clarify the movement and instability of the converging cylindrical shock waves. Experiments were conducted in an annular shock tube of 230 mm o.d. and 210 mm i.d. connected to a cylindrical test section of 210 mm diameter. Double exposure holographic interferometry was used to visualize the converging cylindrical shock waves. Incident shock Mach numbers ranged between 1.1 and 2.0 in air. A numerical simulation was conducted using the TVD finite difference scheme. It was found in the experiments that although the initial shock wave configuration looked cylindrical, it was gradually deformed with propagation towards the center and finally showed mode-four instability. This is attributable to the existence of initial disturbances which were introduced by the struts which supported the inner tube of the annular shock tube. This trend was significant for stronger shock waves indicating that at the last stage of shock wave convergence the initial perturbations of the converging cylindrical shock wave were amplified to form the triple point of Mach reflection. The numerical results correctly predicted the experimental trend.

**Key words:** Converging cylindrical shock wave, Stability, Holographic interferometry, TVD finite difference scheme

## 1. Introduction

Stability of converging cylindrical shock waves is one of the unsolved problems of shock wave dynamics associated with shock wave focusing. Converging cylindrical and spherical shock waves are known to produce high temperatures and pressures at the center of convergence. Recently shock wave focusing has been used for various interesting scientific and engineering applications (Takayama 1990).

The first analytical work concerning converging shock waves was done by Guderley (1942). He obtained a self-similar type solution for the convergence of the cylindrical and spherical shock waves. Experimentally, Perry and Kantrowitz (1951) produced converging cylindrical shock waves using a unique annular shock tube having an axisymmetric tear drop shaped inner core. Since then, many research works have been reported on this problem; experimentally (Wu et al. 1977; Takayama et al. 1987) and theoretically or numerically (Gardiner et al. 1982; Itoh and Abe 1984; Demmig and Hehmsoth 1989; Watanabe 1989). However, the physics of converging shock waves and particularly initiation of instability of the converging shock waves has not yet been clarified, since this behavior is primarily dependent on nonlinear characteristics of shock waves (Watanabe 1989).

In this paper the converging cylindrical shock waves were generated by using a co-axial annular shock tube which had annular structure, similar to that of Perry and Kantrowitz (1951). The co-axial annular shock tube enabled transformation of a planar shock wave to a converging cylindrical shock wave. The whole sequence of shock convergence was successfully visualized with double exposure holographic interferometry. To interprete the experimental results, a numerical simulation, using the TVD finite difference scheme, was conducted and good agreement was obtained between the experiment and numerical simulation. Based on the numerical results, the relationship between intensity of the initial disturbance and shock wave distortion was discussed in some detail.

## 2. Experimental setup

### *2.1. Shock tube and test section*

A 50 mm i.d. shock tube was used to produce planar shock waves. This was connected to a co-axial annu-

*Offprint requests to:* K.Takayama

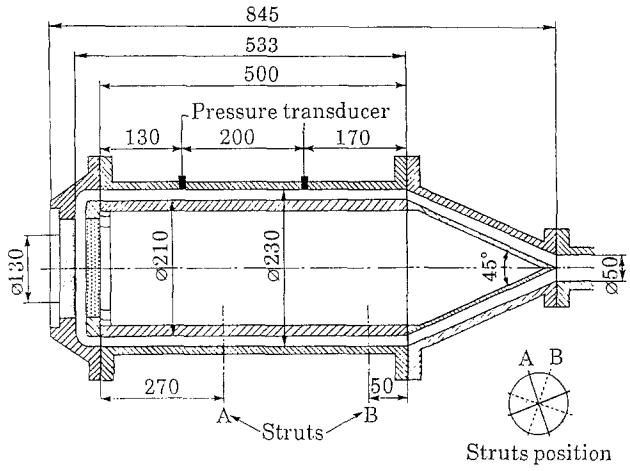


**Fig. 1.** Annular shock tube

lar shock tube. The annular shock tube consisted of two co-axial tubes having an inner and outer diameter of 210 mm and 230 mm, respectively as shown in Fig. 1. The inner tube was supported by two sets of four equiangularly distributed struts from the outer tube and its upstream part had a conical section whose apex angle was 45°. The struts were 18 mm o.d. cylinders. The clearance between the inner and outer tubes was adjusted to be 10.0 ± 0.02 mm. The blockage ratio of the struts to the annular shock tube cross section was 0.12. The co-axial annular section was 500 mm long. It was expected that a longer straight co-axial section was preferable to attenuate the non-uniformities of the shock wave caused by the struts and the cone tip. As a matter of fact, the present longer co-axial section was more effective to attenuate the shock wave than those used in previous works (Perry and Kantrowitz 1951; Wu et al. 1977).

An axisymmetric 90° bend was connected to the end of the co-axial annular section to turn the shock wave into a stabilized converging cylindrical shock wave (Takayama et al. 1987). Configurations of the bend significantly affected the movement and instability of the converging cylindrical shock waves near the center of convergence. In our previous preparatory experiments on shock propagation over two-dimensional 90° bends (Takayama et al. 1977), we found that an optimum 90° configuration existed which smoothly transformed the shock waves and was a smoothly converging and diverging shape. It was also found that a smoothly curved bend was more preferable than a sharp 90° bend. However, in the present series of experiments, a simple smoothly curved bend was used. Then the radial gap between the outer and inner corners of the bend was 10 mm. The radii of the inner and outer corners of the bend were 2.5 mm and 12.5 mm, respectively.

A 130 mm o.d. glass observation window was installed in the outside wall of the test section. A 130 mm o.d. aluminum plated glass mirror was placed on the inside wall, with the coated surface facing the flow. The gap between the mirror and window was 10 mm. For the experiments, the test gas was air at initial pressures that ranged from 5 kPa to 100 kPa. In order to measure the incident shock Mach number, two pressure transducers, Kistler 603B, were placed on the outer annular section at a 200 mm interval. The time differences between these pressure signals were measured with a digital counter and then average shock Mach numbers were calculated. Incident shock Mach numbers ranged from 1.1 to 2.0 in air.

### *2.2. Holographic interferometry*

Figure 2 shows a schematic diagram of the holographic interferometric system which is similar to a conventional shadowgraph method except for the addition of a reference beam. This system was very similar to Twyman-Green interferometry (Takayama 1983). The optical system consisted of two paraboloidal schlieren mirrors of 300 mm diameter and 3 m focal length A, a 6:4 beam splitter which transmits 60 % of light intensity and reflects 40 % of light intensity BS, mirrors M which adjust the light path lengths of the object beam and the reference beam to be as close as possible and lenses L which focus the image of the test section onto a holographic film. By combining different image focus lenses, the magnification of the image of the test section on the film was arbitrarily chosen. In the present experiment it was about 0.5.

A holographic double pulse ruby laser R (Apollo Lasers Inc. 22DH 25 ns pulse duration and 2 J/pulse) was the light source. The ratio of the light intensity of reference and object beams was adjusted to range from 2:1 to 3:1 by using neutral density filters or by changing the angle of the diverging object beam through the beam splitter to the paraboloidal mirror. The angle between object and reference beams was designed to be about 20° and the path difference between these beams was adjusted to be less than 50 mm. The holographic film was 100 mm × 125 mm sheet film, AFGA 10E75. It was processed with Kodak D-19 developer to double exposures for 4.5 min at 293 K and to single exposures for 8 min, fixed with Fuji-super fixer for 5 min and rinsed in running water for 15 min.

In conventional photography, only information of light intensity which was reflected from or transmitted through an object is recorded on the film. Holographic interferometry is a technique in which the phase information of light which was reflected from or transmitted through an object can be recorded, in particular by overexposing the film with the reference beam. When a hologram thus constructed is illuminated again with the reference beam or a beam which can be equivalent to the reference beam, the image of the object is reconstructed as a real or virtual image (Caulfield 1979). To acheive this, a coherent monochromatic light source, a laser beam, is needed. Double exposure holographic interferometry quantitatively enables one to visualize shock wave phenomena. The fringes in a reconstructed holographic interferogram correspond to isopycnics. In

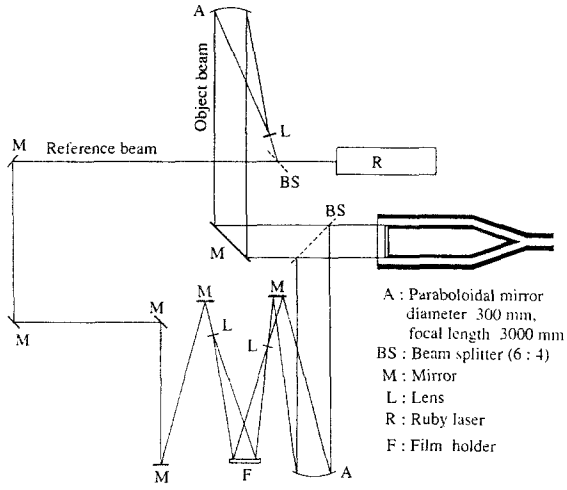


**Fig. 2.** A schematic diagram of the holographic interferometric system

this technique, the first exposure is taken prior to the shock wave arrival at the test section while the second exposure is triggered by the shock wave. The variation of light intensity $I$ and the order of the fringes are correlated to the spatial phase change $\phi(x, y)$ as follows,

$$I \propto \cos \phi(x, y) \tag{1}$$

where $\phi(x, y)$ is the phase change.

Since the object beam was reflected from the mirror on the inner wall and the object beam crossed the test section twice, the sensitivity was doubled.

$$S = \frac{2KL\Delta\rho}{\lambda} \tag{2}$$

where $S$, $K$, $L$, $\Delta\rho$ and $\lambda$ are the fringe number, the Gladstone-Dale constant of 0.225 $cm^3/g$ in air, the width of the test section (10 mm), density variation and wavelength of the light source, respectively. For reconstruction an Argon-Ion laser (514.5 nm wave length and 1 W) was used. The distortion of reconstructed images due to the difference of wave length of the light between the experiment and reconstruction of holograms and also the difference of the optical arrangement between the experiment and reconstruction was negligibly small.

## 3. Numerical simulation

The TVD finite difference scheme (Harten 1983; Itoh and Takayama 1987) was applied to the two-dimensional unsteady Euler equations. Two computational models were considered as shown in Fig. 3a.

### *3.1. Computational model*

#### 3.1.1. Simulation–1

The computational region was the axisymmetric 90° bend and the convergence region. However, in this model

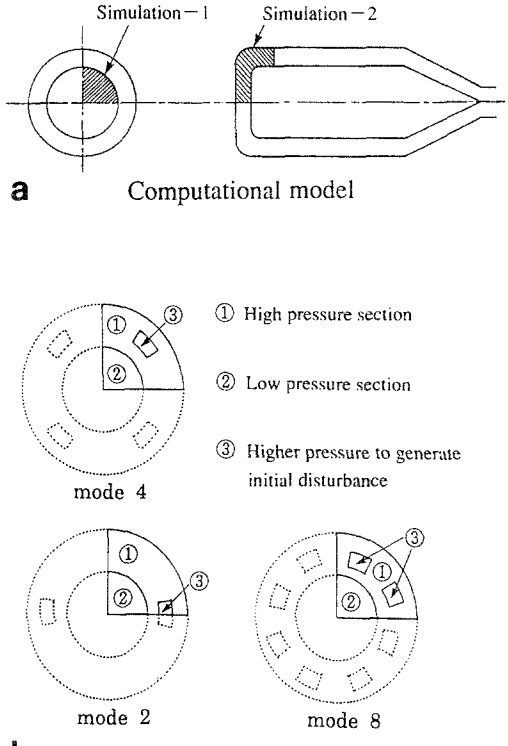


**Fig. 3.** Region of numerical simulation

no initial disturbances were considered, the computation was intended to predict the shock wave movement in the 90° bend and shock wave convergence in the test section. The initial shock Mach number ranged from 1.1 to 2.0.

#### 3.1.2. Simulation–2

In this simulation, only the circular convergence region was considered and initial disturbances were superimposed on the high pressure section and their influence on shock convergence was examined.

#### 3.1.3. Basic equations

The conservation form of the Euler equations for inviscid compressible flow in Cartesian coordinates $(x, y)$ can be expressed in general curvilinear coordinates $(\xi, \eta)$ as,

$$\frac{\partial \hat{\boldsymbol{U}}}{\partial t} + \frac{\partial \hat{\boldsymbol{F}}}{\partial \xi} + \frac{\partial \hat{\boldsymbol{G}}}{\partial \eta} + \hat{\boldsymbol{W}} = 0 \tag{3}$$

where the vector $\hat{\boldsymbol{U}}$ represents the conserved quantities, $\hat{\boldsymbol{F}}$ and $\hat{\boldsymbol{G}}$ represent numerical fluxes, and $\hat{\boldsymbol{W}}$ represents an inhomogeneous term in the axisymmetric flow.

$$\hat{\boldsymbol{U}} = \frac{\boldsymbol{U}}{J}, \quad \hat{\boldsymbol{F}} = \frac{1}{J}(\xi_x \boldsymbol{F} + \xi_y \boldsymbol{G})$$
$$\hat{\boldsymbol{G}} = \frac{1}{J}(\eta_x \boldsymbol{F} + \eta_y \boldsymbol{G}), \quad \hat{\boldsymbol{W}} = \frac{\boldsymbol{W}}{J} \tag{4}$$

where $J$ is the Jacobian given as,

$$J = \xi_x \eta_y - \xi_y \eta_x. \tag{5}$$

$$\boldsymbol{U} = \begin{bmatrix} \rho \\ \rho u \\ \rho v \\ e \end{bmatrix}, \quad \boldsymbol{F} = \begin{bmatrix} \rho u \\ \rho u^2 + p \\ \rho uv \\ (e+p)u \end{bmatrix}, \quad \boldsymbol{G} = \begin{bmatrix} \rho v \\ \rho uv \\ \rho v^2 + p \\ (e+p)v \end{bmatrix}, \tag{6}$$

$$\boldsymbol{W} = \begin{bmatrix} \rho u/x \\ \rho u^2/x \\ \rho uv/x \\ (e+p)u/x \end{bmatrix}$$

where $p$, $\rho$, $u$, $v$, and $e$ are the pressure, density, $x$-component velocity, $y$-component velocity and total energy per unit volume, respectively. In simulation-2, the inhomogeneous term $\boldsymbol{W}$ in (6) was excluded from the basic equations. However, the simulation was conducted in cylindrical coordinates.

For a perfect gas the pressure is given by

$$p = (\gamma - 1)\{e - \frac{\rho}{2}(u^2 + v^2)\} \tag{7}$$

where $\gamma$ is the ratio of specific heats and is constant, since real gas effects are neglected.

However, when the transmitted shock arrives very close to the center, it becomes so strong that real gas effects will become significant. The influence of ionization on a converging strong Argon shock was studied numerically by Demmig and Hehmsoth (1989).

### *3.2. Initial conditions*

In simulation–1, the initial Mach number ranged from 1.1 to 2.0 to match the experimental conditions. The normal incident shock just upstream of the 90° bend was taken as the initial condition. 351 × 25 grid points were used.

In simulation–2, this is equivalent to a cylindrical imploding shock tube problem having high pressure regions distributed around the outer boundary as shown Fig. 3b. The computational domain was a quarter section of the circular flow field. The high pressure section is assumed to be initially isothermal. The ratio of the high pressure to the initial low pressure was 10. The initial disturbance was given by excess pressure variations which were expected to simulate the inflence of the disturbances caused by the struts. However, the present numerical model was fictitious since there is no cylindrical diaphragm which can be ruptured simultaneously in space and time. Nevertheless this model was useful to interpret the onset of instabilities. The numerical simulation was carried out for initial excess pressures of 10 %, 50 % and 200 %, respectively. Mode numbers, m = 2, 4 and 8 were studied. 401 × 151 grid points were used.

## 4. Results and discussion

### *4.1. Interferograms*

Sequential interferograms are shown in Fig. 4. For each Mach number, several experiments were repeated with identical initial condition. The repeatability of the incident shock Mach number was maintained within ±2.5 % for each nominal incident Mach number. Figures 4a-d, 4e-h and 4i-m show reconstructed infinite fringe interferograms for $M_s$ = 1.1, 1.5 and 2.0, respectively. The displayed elapsed time started when the transmitted shock wave passed the first pressure gauge, as seen in Fig. 1.

#### 4.1.1. $M_s = 1.1$

In Fig. 4a, a 16 mm diameter cylindrical shock wave converged towards the center. Although the shock wave looked cylindrical, behind it a slight non-uniformity existed since the fringe distribution was not cylindrical. The fringe distribution were quadrangularly disturbed which indicated the onset of mode-four instability. In Fig. 4b, the shock wave was no longer cylindrical but was deformed, and the flow non-uniformity behind the shock wave became even more pronounced. The fringes looked like a four-leaf clover. One fringe shift corresponds to a density change of about 12 % of the standard condition. In Fig. 4c, as the shock wave propagated towards the center, the four-leaf clover shape became much clearer and showed that the density non-uniformity was enhanced. It was found that the position of these clover leaves was directed to the position of the 4 struts located in section A in Fig. 1.

Initially the effect of the disturbances caused by the struts on the shock wave and the flow field behind it was small as seen in Fig. 4a, however this effect was amplified as the shock wave converged in Fig. 4c. Figure 4d shows the reflected shock wave which becomes cylindrical with propagation outward and is known to be stable. Behind the reflected shock wave, the pressure and density is nearly uniform so that few fringes can be seen. Near the convergence center a small cross shape can be seen. This is, as explained later, due to the remaining vortices. The vortices were produced by the three shock confluences and were evidence that Mach reflection occurred near the center. Perry and Kantrowitz (1951) visualized shock convergence by shadowgraph and concluded from their photographs that weak shock convergence was stable. However, in Figs. 4c and 4d the converging shock wave could not be cylindrical and the vortices remained behind the reflected shock wave. This indicates that the converging shock wave was *not* stable even for $M_s$ = 1.1.

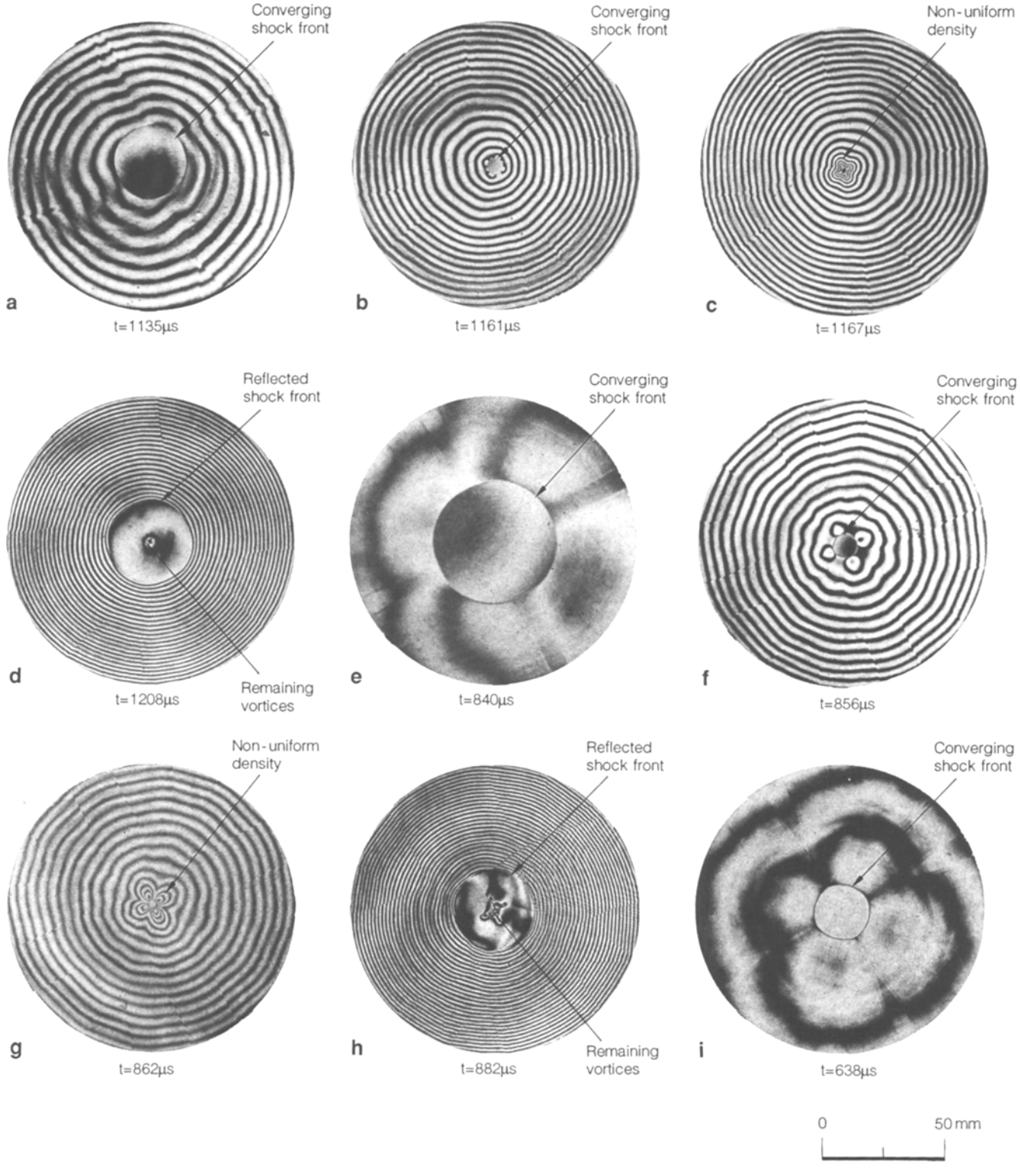
Converging shock front
a
t=1135μs
Converging shock front
b
t=1161μs
Non-uniform density
c
t=1167μs
Reflected shock front
Remaining vortices
d
t=1208μs
Converging shock front
e
t=840μs
Converging shock front
f
t=856μs
Non-uniform density
g
t=862μs
Reflected shock front
Remaining vortices
h
t=882μs
Converging shock front
i
t=638μs
0
50 mm

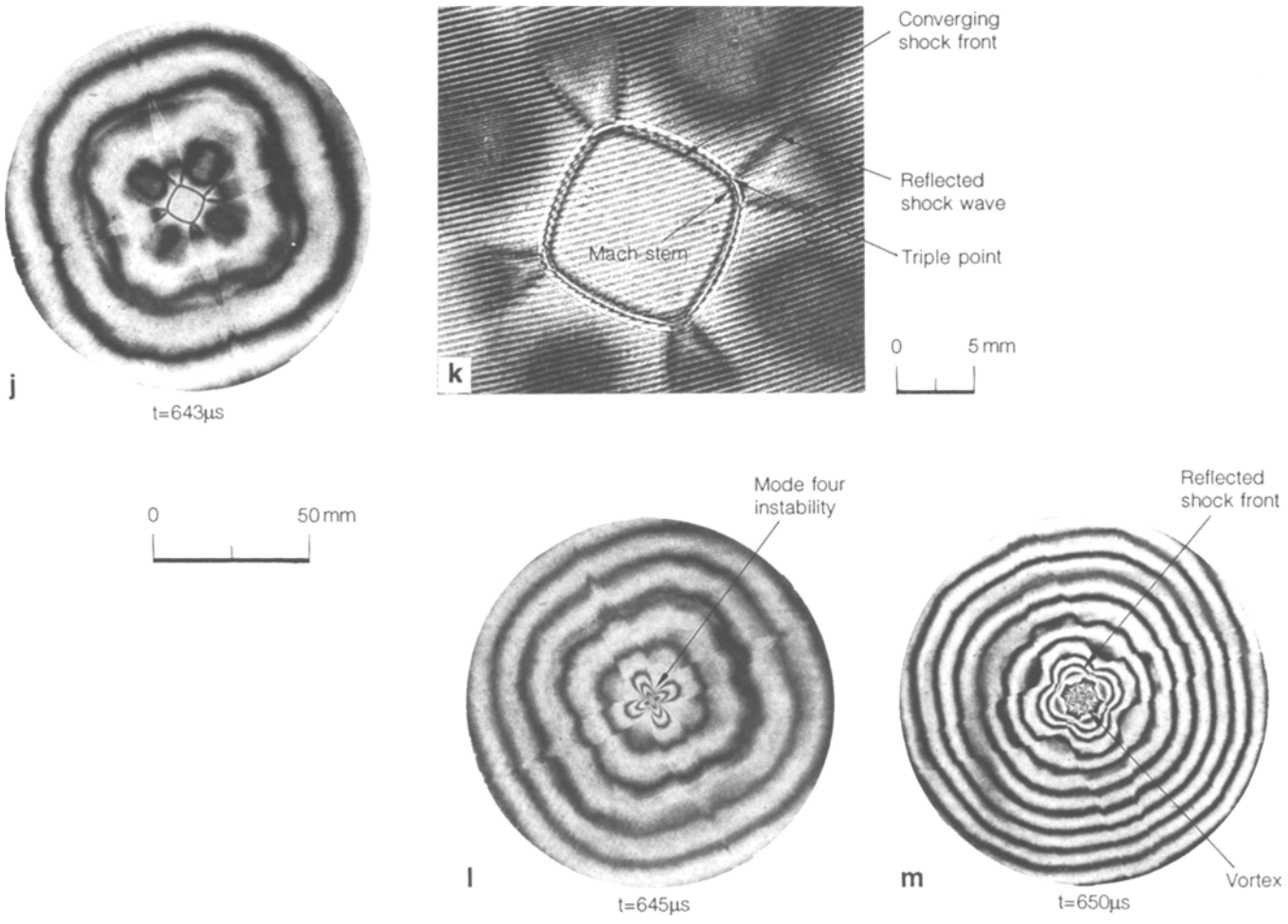


**Fig. 4a-m.** Interferograms, a-d; $M_s = 1.1$, e-h; $M_s = 1.5$, i-m; $M_s = 2.0$

4.1.2. $M_s = 1.5$

In Fig. 4e, at an earlier stage, the converging cylindrical shock wave with 27 mm diameter is nearly cylindrical. Although in Figs. 4e-h, similar to Figs. 4a-d, the converging shock wave was initially nearly cylindrical, it was, with convergence towards the center, more significantly disturbed again with mode-four instability. The shock wave very close to the center looked square as seen in Fig. 4f. Being initially negligibly small, the shock deformation grew larger with propagation.

However, the shock deformation can not grow infinitely large and still be continuous. The large and continuous shock deformation induced, large and continuous changes of flow variables along the shock front. However, this could not be true if the gradient of the flow variables became very large along the shock front. The large shock deformation, finally could not to be continuous and the transition to Mach reflection occurred. In Fig. 4g, the larger shock deformation terminated and the triple points having a familiar three shock confluence composed of an incident shock, a reflected shock, a Mach stem and a slip line are formed. This tendency was even more significant for stronger shock cases, for example $M_s = 2.0$.

Figure 4h shows the reflected shock wave from the center. When the mode-four instability terminated and Mach reflection appeared, consequently at the triple points, the four pairs of slip lines or vortices appeared. These vortices collided mutually at the center and stayed at the center since the particle velocity behind the reflected shock was so small. Similar phenomena existed in shock focusing experiments. When a planar shock wave reflected from a concave wall, the shock transition from Mach to regular reflection occurred along the concave wall. The regular reflection which was an outcome of the inverted Mach reflection, accompanied the secondary triple point and a vortex. The secondary triple points behind regular reflections on the upper and lower walls collided and at the focus region of the concave

wall, the two secondary triple points and vortices from the upper and lower concave walls collided with each other and remained there. The final interaction of the secondary triple points and vortices formed a mushroom shape (Takayama and Ben-Dor 1986). Similarly in this case the four pairs of vortices finally formed a shape which looked like cross shaped mushrooms. It was concluded that the remains of the vortices at the center indicated that the converging cylindrical shock having larger deformation finally converted into Mach reflection. In previous converging cylindrical shock experiments (Perry and Kantrowitz 1951), shadowgraphs showed vortices which looked very irregular at the center of convergence even for weak shock waves. This again indicated that converging cylindrical shock waves were unstable.

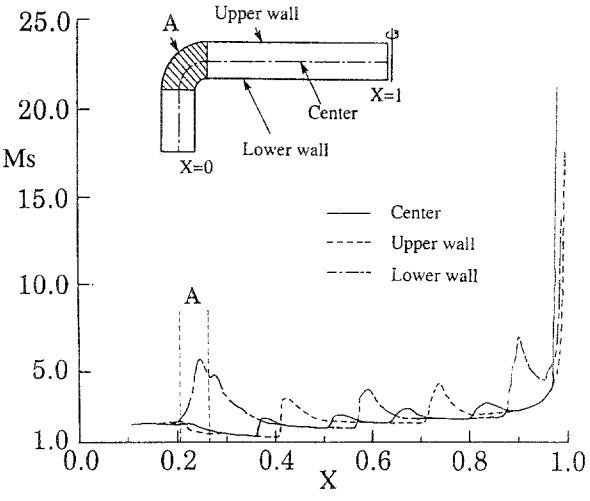


**Fig. 5.** Shock Mach number variation

4.1.3. $M_s = 2.0$

In Fig. 4i, an already slightly disturbed cylindrical shock of mean diameter of about 12 mm converges towards the center. For this stronger shock wave case, the shock wave became non-cylindrical at a much earlier stage. The non-cylindrical deformation of the shock wave was again attributable to shock interaction with the struts which supported the inner co-axial annular tube. In weaker shock waves these disturbances seemed to be well suppressed, especially at the earlier stage but in the stronger shock case they always remained in the shock wave. In Fig. 4j they turned into Mach reflection. The three shock confluences, i.e. the converging cylindrical shock as an incident shock, the reflected shocks, straight Mach stems and slip lines were clearly seen.

Figure 4k is a blow-up of the Fig. 4j. As marked, we can easily see the three shock confluence. Since in previous experimental work, shadow or schlieren methods were mainly used, the non-uniformity of the flow behind the converging cylindrical shock wave was not easily detectable. It should be noted again that the present holographic interferometer was particularly useful to detect the earliest onset of instability in the flow preceding the deformation of the shock wave. In Fig. 4k, once the Mach reflections appeared, the triple point was self preserved. These three shock confluence were predictable by solving the Rankin-Hugoniot relation for oblique shock waves. Figure 4k shows a typical mode-four instability. In Fig. 4m, the reflected shock wave diverged from the center and was again stable even for strong shock waves.

*4.2. Influence of the bend*

Figure 5 shows, for simulation–1, a numerical result of shock Mach number variation along the outer and inner walls and also along the center line of the 90° bend for $M_s = 2.0$. In Fig. 5, the ordinate is shock Mach number and the abscissa is a nondimensional distance along the bend, the origin O corresponds to the upstream uniform condition of the bend and the convergence center is designated as 1. Along the outer and inner walls and also along the center line, the shock Mach number increased with shock convergence. However, the shock Mach number did not vary monotonically but maxima existed during the convergence process. These maxima indicated that the shock wave was locally accelerated and decelerated repeatedly due to the fact that, after the incident shock wave passed through the 90° bend, the transmitted shock wave was reflected and diffracted between the upper and lower walls of the test section. The triple point on the transmitted shock, the so-called shock-shock, moved along the shock wave and was reflected repeatedly between upper and lower walls. Therefore, the slip lines which were remaining in the test section looked like zig-zag shapes. This trend was clearly observable in previous two-dimensional shock tube experiments (Takayama et al. 1977). The shock Mach number distributions along the outer and inner walls shows several peaks.

In the present holographic flow visualization, the converging shock wave was observed to have plausible thickness. This is attributable to the fact that the triple point exists on the converging shock wave and consequently the converging shock is curved. Therefore, when the collimated light passed through the test section parallel to the shock wave, the deformed shock was observed to be thickened. This indicated that in using the annular shock tube, the cylindrical shock convergence process could be slightly three-dimensional. Therefore, the model in simulation–2 illuminated an example of simplified characters of the converging cylindrical shock waves.

In the infinite fringe holographic interferograms, each fringe corresponds to isopycnics. Therefore, it is possible experimentally to evaluate the density distributions by counting fringe numbers as shown in Eq. (2). The evaluated densities from the interferograms were compared with the computational isopycnics. Good agreement was obtained between the experiment and the computation but only in the vicinity of the convergence center. How-

ever, it was found that agreement was poorer outside the convergence center. A number of false fringes existed in the interferograms. The false fringes did not correspond to the density variation but were thought to be caused by vibration of the test section which was induced when the incident shock hit the inner core of the annular section and consequently due to the surface deformation of the test section. As seen in Figs. 4, the false fringes increased in number with elapsed time. Unfortunately at the moment we are unable to separate these false fringes from the real density variation which were generated by the shock and the flow in the test section.

### *4.3. Pressure distribution*

Figures 6a, 6b and 6c show pressure measurements for $M_s$ = 1.1, 1.5 and 2.0, respectively. The pressure was measured 15 mm, 30 mm and 45 mm from the center. The pressure transducers, Kistler 603B had a 2.5 mm diameter pressure sensitive area and were placed on the outer wall of the test section. The experimental results were compared with the numerical simulations. Computational pressure histories at these points were evaluated by integrating the computational pressures over several grid points which corresponded to an area equivalent to the sensitive area of the pressure transducers. Good agreement was obtained between the experiment and the computation. However, the computational maximum pressures differ marginally from the experimental results, since in the present computation the initial disturbances were neglected and viscosity was not taken into account.

### *4.4. Numerical simulation with initial disturbances*

Figure 7 shows the isopycnics for $M_s$ = 2.0 obtained in simulation-2 and with an initial excess pressure of 100 %. In experiments, positions of triple points were maintained in an angular sense. In the numerical simulation in Figs. 6b and 6c, triple points collided mutually and reflected as if the triple points were moving in a circumferential direction. The isopycnics which looked like four-leaf clover shapes also looked to be rotating. It is somehow different to compare the present numerical results with the experimental result in Fig. 4, simply because there are some differences in initial conditions between the experiment and the simulation. However, it is clear that the initial disturbance are amplified with shock convergence and finally turn into Mach reflection.

Figure 8 shows the pressure distribution along the shock front for various initial disturbances, that is, initial excess pressures. The ordinate is pressure ratio referred to the initial pressure and the abscissa is the circumferential angle. In Fig. 8a, the converging shock waves were not significantly disturbed but the pressure behind it was gradually enhanced with propagation. At $t_5$ = 72 $\mu s$, only the reflected shock showed some non-uniformity. In Fig. 8b, the excess pressure is 50 %,

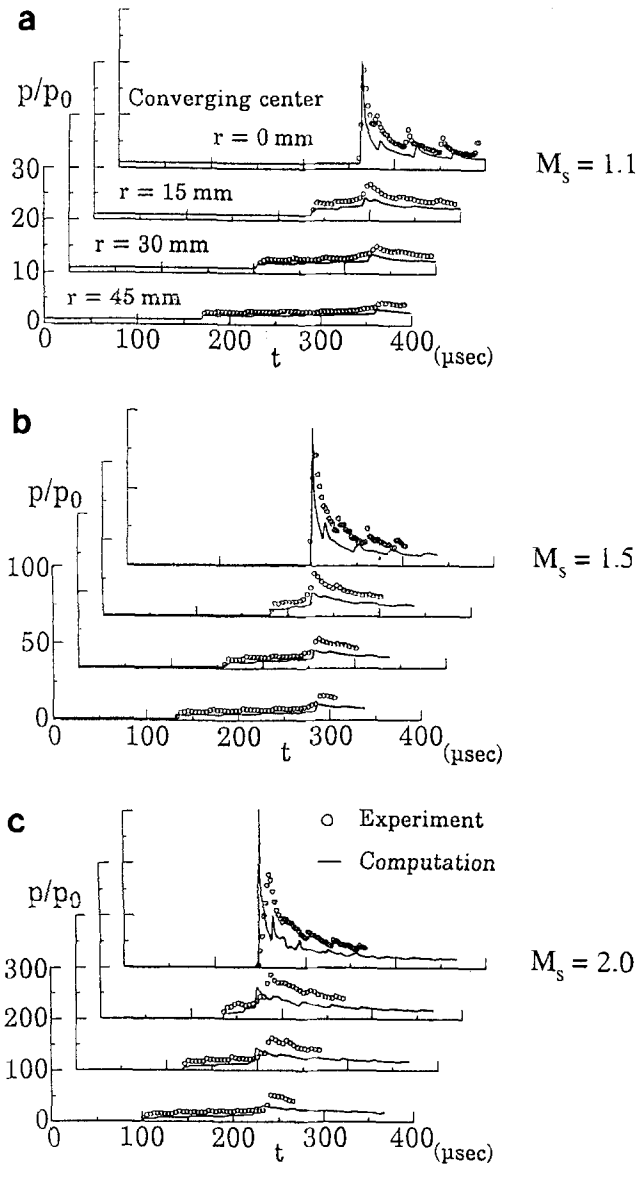


**Fig. 6a-c.** Pressure mesurements, a; $M_s$ = 1.1, b; $M_s$ = 1.5, c; $M_s$ = 2.0

the initial disturbance propagated circumferentially and was amplified. The broken line in Fig. 8b shows a trajectory of the non-uniform part which is initially moving outwards and then reflected by accompanying the distinct pressure jumps. This means that Mach reflection occurred. It is found that high overpressure appeared at the converging center. This trend was also seen in Fig. 5 where the shock converged at the center.

Comparatively uniform pressure appeared behind the reflected shock which agreeed well with the experiment, since in the experiment only a few fringe shifts existed behind the reflected shock. In Fig. 8c, in the case of 200 % of excess pressure, a drastically sharp pressure rise was seen which corresponded to the formation of Mach reflection as seen in Fig. 4i-m. It was found that the bigger the initial disturbance is, the higher the peak pressure ratio is. For a given initial shock Mach number

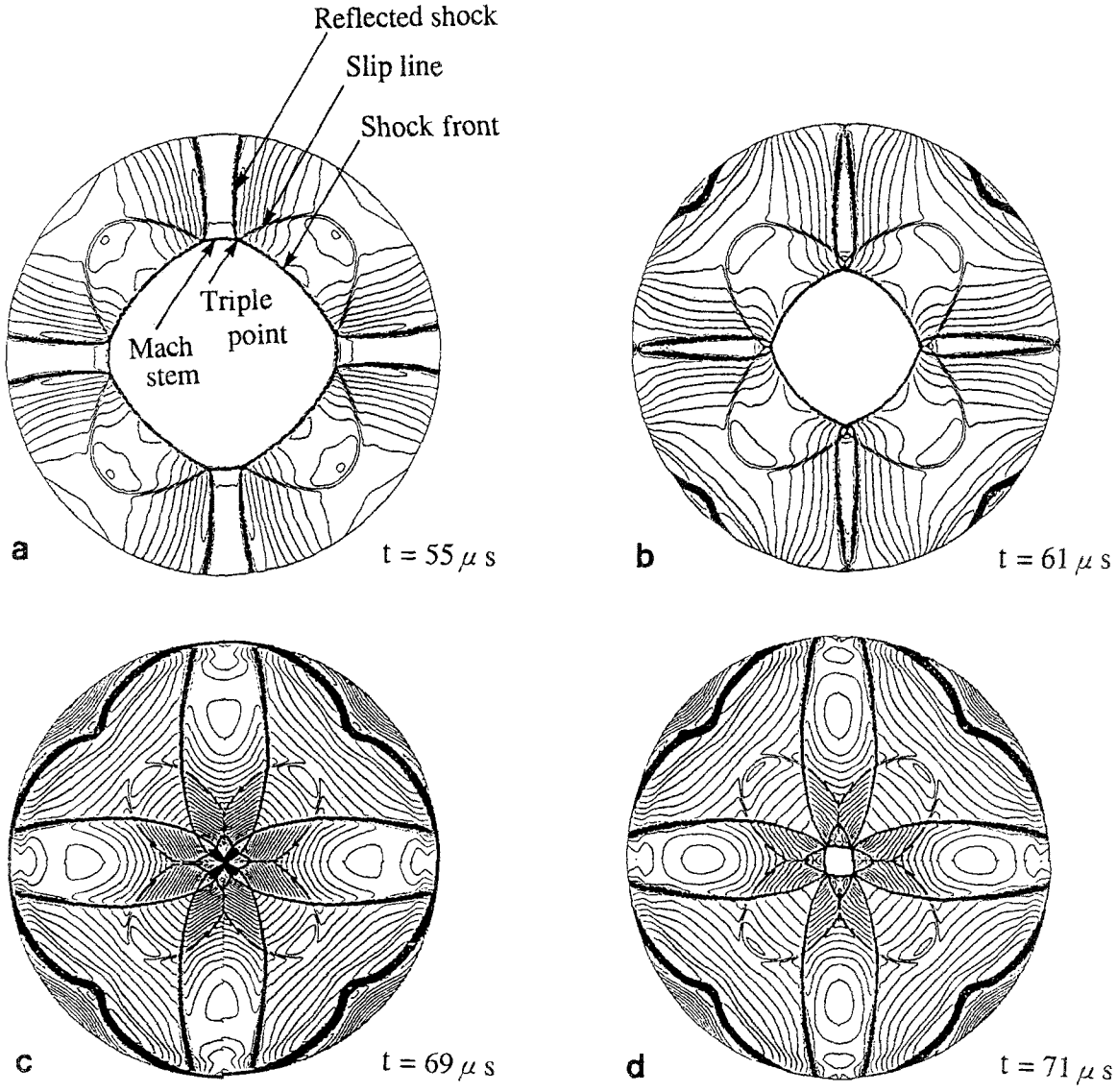


**Fig. 7a-d.** Isopycnics, Mode = 4, a; $t = 56$ $\mu$s, b; $t = 63$ $\mu$s, c; $t = 70$ $\mu$s, d; $t = 72$ $\mu$s

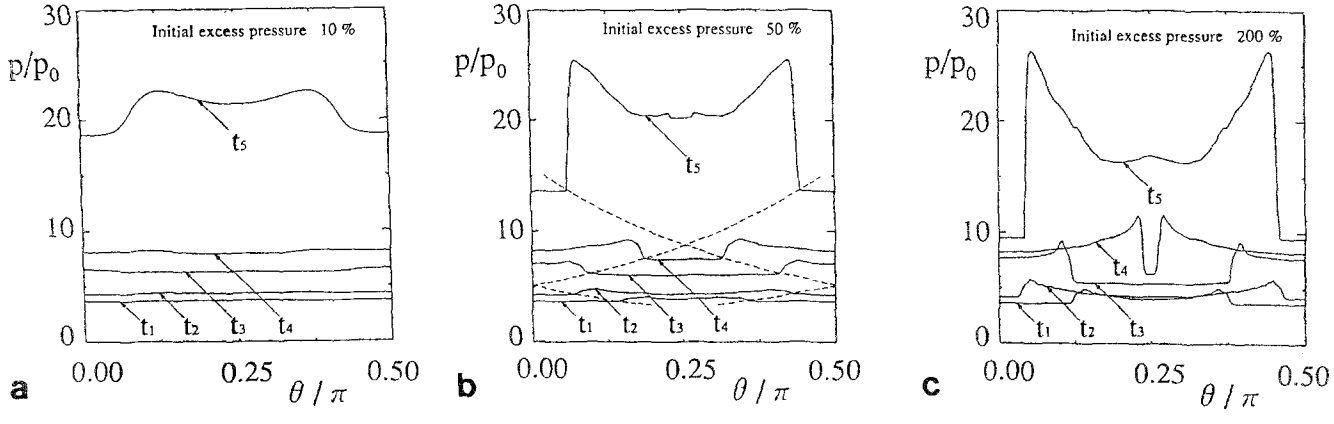


**Fig. 8a-c.** Pressure distribution, $T_1 = 44$ $\mu$s, $T_2 = 56$ $\mu$s, $T_3 = 68$ $\mu$s, $T_4 = 70$ $\mu$s, $T_5 = 72$ $\mu$s

with a small initial disturbance, this averaged pressure along the shock front was enhanced and its distribution became comparatively uniform. When the initial disturbance was larger, the averaged pressure along the shock wave was not as high as the weak initial disturbance case but the peak pressure at the center was enhanced.

The four struts at B in Fig. 1 also contributed to the final instability mode. However, as mentioned above, the instability caused by stronger initial disturbances grew faster than by weaker the ones. As the disturbances caused by the struts in position B were attenuated with propagation more quickly than those by the struts from position A. Therefore, the contributions by the struts in the position B became negligibly small to the final instability mode and only the influence from the struts in position A were dominating to the final instability mode.

### *4.5. Shock wave distortion*

#### 4.5.1. Measurement from interferograms

In ideal cylindrical shock convergence, the cylindrical shape was always maintained and the final shock convergence at the center produced high pressure and temperature. However, it is not easy to achieve this condition physically. In the present series of experiments, we saw that the initial disturbance of the shock wave, however small it may have been, was gradually amplified with convergence. Figures 9a-c, d-f and g-i show distortions of the converging shock waves from the cylindrical shape, which were evaluated from the interferograms shown in Fig. 4, for $M_s = 1.1$, 1.5 and 2.0, respectively. The ordinate is the deviation $\Delta R$ of a deformed shock wave from its averaged radius $R_a$ normalized with mean radius of the converging shock. The abscissa is the circumferential angle $\theta/2\pi$. The deviation of the radii was found to always have four coherent peaks. The four peaks grew with shock convergence. This is due to the growth of the mode-four instabilities associated with the struts. Small initial disturbances caused by the struts were transfered to the test section and at an earlier stage, deformed very slightly, the cylindrical shock wave. This instability grows with shock convergence. For $M_s = 1.1$ the initial deformation was so small that at this stage the shock wave was cylindrical as shown in Fig. 9a. However, shock deformation grows later to a noticeable level as shown in Fig. 9c.

For $M_s = 1.5$, this trend was more pronounced. The initial disturbances already existed at $R_a = 27$ mm and were gradually amplified as shown Figs. 9d-f. The typical example was seen in Figs. 9g-i for $M_s = 2.0$. The small deformation grew to the extent that small perturbation theory does not apply. The larger deformation of the converging shock wave finally formed the Mach reflection. In Fig. 9i, the flat topped shock deformation clearly indicated discontinuities of the Mach reflection as seen in Fig. 4k. It is concluded that the converging cylindrical shock wave is unstable even for weak shock waves and the initial small shock deformation grew with shock convergence and resulted in the deterministic nonlinear behavior of triple point formation. The present sequential observation of shock deformation can be used directly to obtain time and spacial variations of the flow properties behind the converging shock.

#### 4.5.2. Amplification

Figure 10 summarizes the amplification of the shock wave distortion. The experimental results were taken from Fig. 9. The ordinate is $\Delta R/R_a$, deviation of the shock wave $\Delta R$ normalized with mean radius of the converging shock $R_a$ and the abscissa is the mean radius $R_a$ normalized with the characteristic length which is the radius of the observation section $R_d = 65$ mm. In Fig. 10 a small shock deformation existed and increased rapidly when the shock wave was inside the range $R_a/R_d > 0.2$. This change of deviation of the radius was related to the transformation of small perturbations to the triple point. Further it is found that the dimensionless shock deformation seems to be independent of the incident Mach number. The solid line is an empirical curve fit.

The effect of mode numbers of 2, 4, and 8 on the amplification of the shock deformation is compared in Fig. 11. $\Delta R/R_a$ is plotted against the mean radius $R_a/R_d$. It is readily seen that there is a trend that the smaller the mode number, the larger the shock deformation is when the shock travels inside the range $R_a/R_d < 0.5$. However, the trend was not consistent between the modes 2 and 4 at $R_a/R_d = 0.01$. This is because the present computational evaluation of shock deformation became less accurate when the shock was at $R_a/R_d = 0.01$ as the corresponding shock radius was 0.65 mm. This was nearly beyond the limit of the present computational resolution. In the present computation the initial excess pressure for all the initial disturbances for mode numbers 2, 4 and 8 was 100 %.

Therefore, as seen in Fig. 11, if various mode numbers having non-equal initial disturbances coexisted, a smaller mode number and larger initial disturbance would contribute to the final disturbance more strongly than any other combinations of mode number and initial disturbance. In our experiments (Takayama et al. 1987) in addition to the two pairs of 4 supporting struts, twelve pins of 4 mm diameter were placed equiangularly at the 90° corner and the shock convergence was again observed by double exposure holographic interferometry. We saw that at first a mode-twelve instability appeared immediately after the 90° corner. However, carefully observing the interferometric fringes near the center at the final stage of convergence, we found that the mode-twelve instability merged into a mode-four instability. That is, overlapping with the remaining fringes of the mode-twelve instability, again a mode-four instability became dominant. The present numerical study can explain our

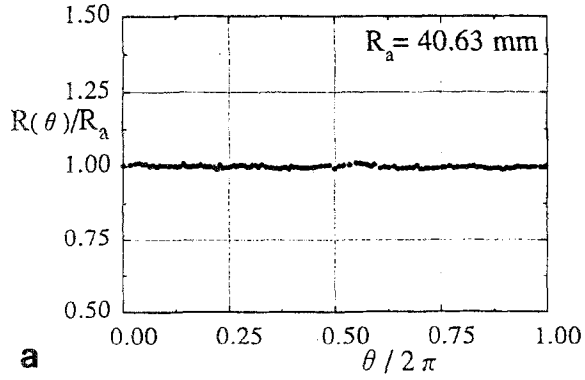


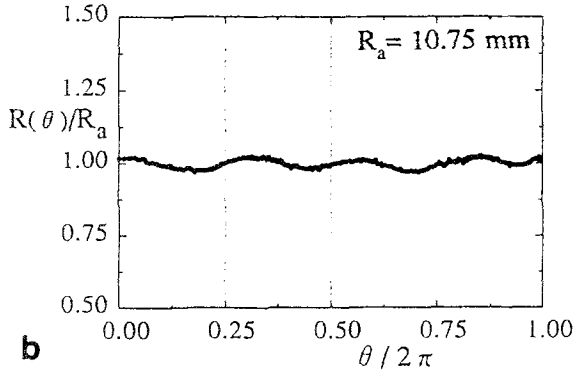


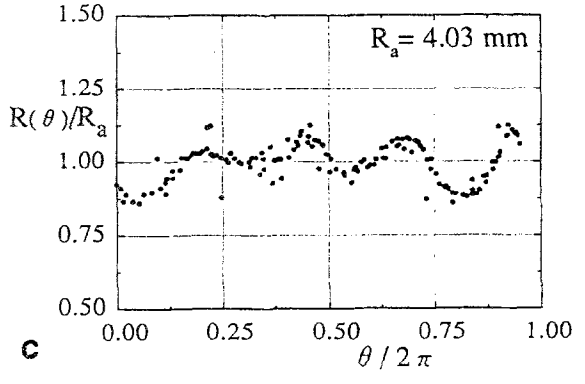


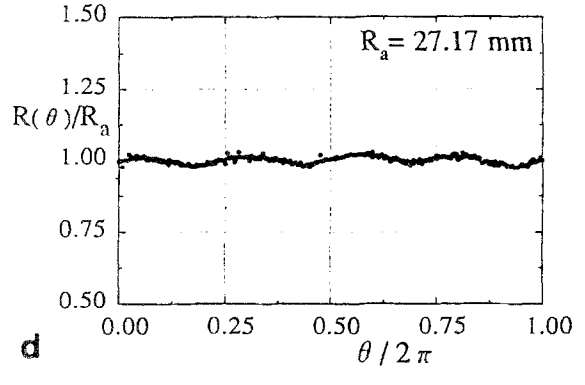


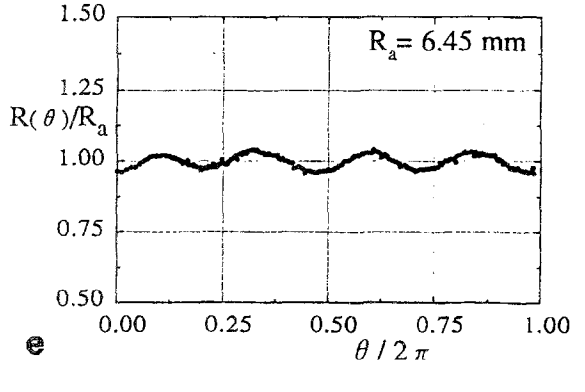


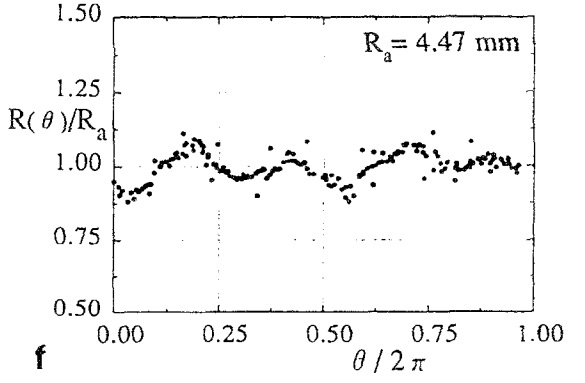


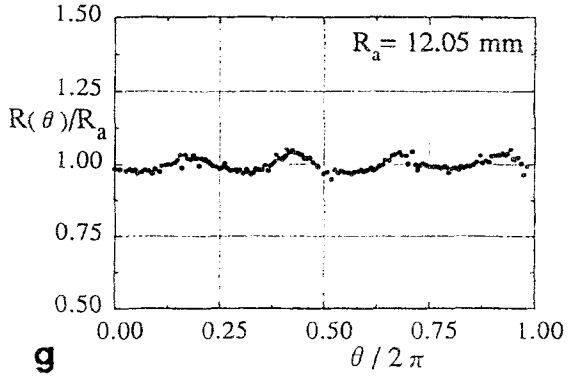


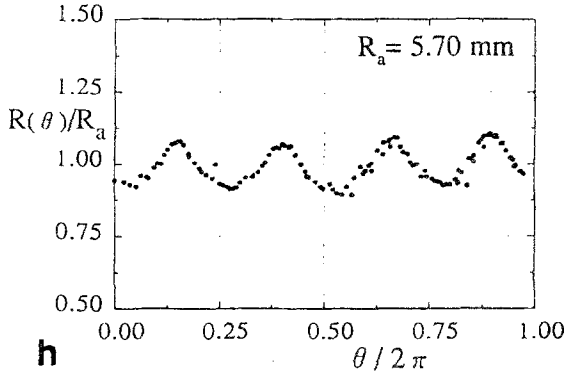


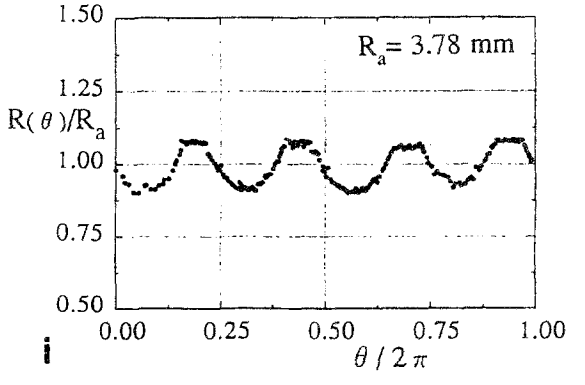


**Fig. 9a-i.** Distortion of the converging cylindrical shock wave, a-c; $M_s = 1.1$, d-f; $M_s = 1.5$, g-i; $M_s = 2.0$

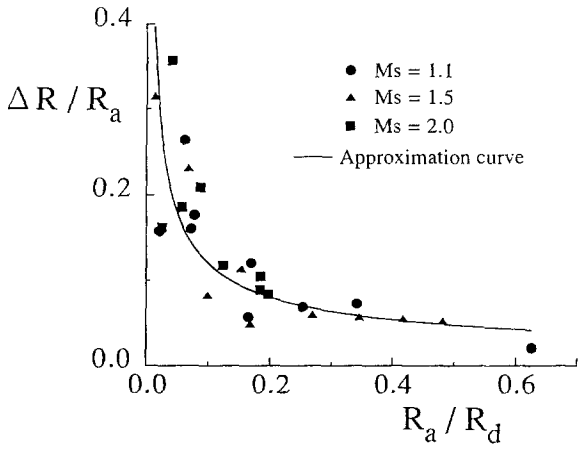


**Fig. 10.** Amplification of the shock front distortion in experiments

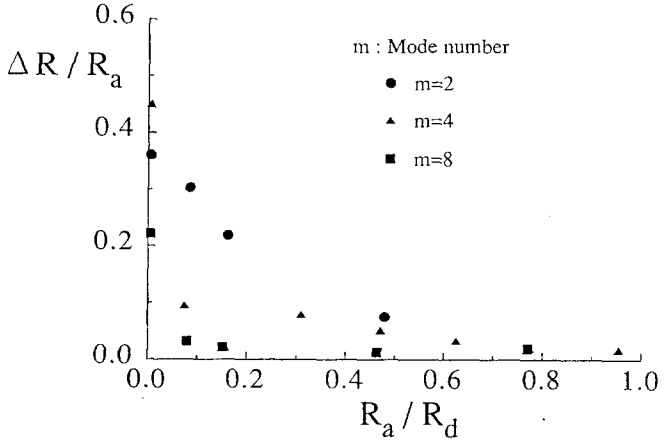


**Fig. 11.** Amplification of the shock front distortion with an excess pressure of100 %, numerical simulation

previous observation of why the mode-four instability having a stronger initial disturbance overtook the weaker mode-twelve disturbances.

## 5. Conclusions

The results obtained are summarized as follows;

*1.* Holographic interferometry is particularly useful to observe the early onset of instability in the flow field preceding the deformation of the shock wave.
*2.* Initial small perturbations of the shock wave grew with shock propagation and, at the final stage, resulted in the formation of triple points.
*3.* Following the convergence, the flow non-uniformity behind the shock wave showed the onset of a mode-four instability which was due to the struts supporting the inner tube of the annular shock tube.
*4.* The bigger the initial disturbance is and the smaller the mode number is, the bigger the amplification of the shock wave distortion is.

*Acknowledgements.* The authors would like to express their gratitude to Messrs. O. Onodera, S. Tomita and H. Ojima of the Shock Wave Research Center of the Institute of Fluid Science, Tohoku University, for their assistance in conducting the present experiments. The authors also gratefully acknowledge Messrs. S. Hayasaka of the machine shop of the institute of Fluid Science, Tohoku University, and K. Takahashi of the Shock Wave Research Center of the Institute of Fluid Science, Tohoku University, for manufacturing the shock tube. The present research was in part supported by the Grant-in-Aid of Scientific Research on Priority Areas, Shock Waves (1990), the Ministry of Education, Science and Culture, of Japan

## References

Caulfield HJ (1979) Handbook of optical holography. Academic Press New York

Demmig F, Hehmsoth HH (1989) Model computation of converging cylindrical shock waves: Initial configurations, propagation, and reflection. In: Kim YM (ed) Proc 17th Int Symp Shock Wave and Shock Tube, pp 155-160

Gardner JH, Book DL, Bernstein IB (1982) Stability of imploding shocks in the CCW approximation. J Fluid Mech 114:41-58

Guderley G (1942) Starke kugelige und zylindrische Verdichtungsstösse in der Nähe des Kugelmittelpunktes bzw. der Zylinderachse. Luftfahrtforsch 19:302-312

Harten A (1983) High resolution scheme for hyperbolic conservation law. J Comp Phys 49:357-393

Itoh T, Abe K (1984) Simulation of instability of cylindrically converging shock waves. In: Proc 4th Int Conf Applied Numerical Modelling, Taiwan, pp 666-671

Itoh K, Takayama K (1987) Transonic shock tube flow over an NACA 0012 aerofoil and elliptical cylinders. In: Bershader D, Hanson RK (eds) Proc 16th Int Symp Shock Tubes and Waves, Stanford Univ Press Stanford, pp 693-699

Perry RW, Kantrowitz A (1951) The production and stability of converging shock waves. J Appl Phys 22:878-886

Takayama K, Kleine H, Grönig H (1987) An experimental investigation of the stability of converging cylindrical shock waves in air. Exp Fluids 5:315

Takayama K, Ben-Dor G (1986) Reflection and diffraction of shock waves over a circular concave wall. Rept Inst High Speed Mech, Tohoku Univ 51:43-52

Takayama K (1983) Application of holographic interferometry to shock wave research. Proc. SPIE 398 pp 174-181

Takayama K, Honda M, Onodera O (1977) Shock propagation along 90 ° bends. Rept Inst High Speed Mech, Tohoku Univ 35:83-102

Takayama K (1990) Proceedings of international workshop on shock wave focusing, Shock Wave Research Center, Institute of Fluid Science, Tohoku Univ

Watanabe M (1989) Stability of converging cylindrical shock wave. Master Thesis, Tohoku Univ in Japanese

Wu JHT, Neemeh RA, Ostrowski PP, Elabdin MN (1977) Production of converging cylindrical chock waves by finite element conical contraction. In: Hertzberg A, Russell D (eds) Proc 11th Int Symp Shock Tubes and Waves, Washington Univ Press Seattle, pp 107-112

This article was processed using Springer-Verlag TEX Shock Waves macro package 1990.